Nuclear Engineering and Technology 54 (2022) 72–83

Contents lists available at ScienceDirect

Nuclear Engineering and Technology

journal homepage: www.elsevier.com/locate/net

Original article

Numerical study on thermal-hydraulics of external reactor vessel cooling in high-power reactor using MARS-KS1.5 code: CFD-aided estimation of natural circulation flow rate

Min Seop Song [a], Il Woong Park [b], Eung Soo Kim [a], Yeon-Gun Lee [c, *]

[a] Department of Nuclear Engineering, Seoul National University, 1 Gwanak-ro, Gwanak-gu, Seoul, 08826, Republic of Korea
[b] Institute for Nuclear Science and Technology, Jeju National University, 102 Jejudaehak-ro, Jeju-si, Jeju, 63243, Republic of Korea
[c] Department of Nuclear and Energy Engineering, Jeju National University, 102 Jejudaehak-ro, Jeju-si, Jeju, 63243, Republic of Korea

ARTICLE INFO

Article history:
Received 27 April 2021
Received in revised form
19 June 2021
Accepted 21 July 2021
Available online 22 July 2021

Keywords:
External reactor vessel cooling
Natural circulation flow
MARS-KS1.5
CFD analysis

ABSTRACT

This paper presents a numerical investigation of two-phase natural circulation flows established when external reactor vessel cooling is applied to a severe accident of the APR1400 reactor for the in-vessel retention of the core melt. The coolability limit due to external reactor vessel cooling is associated with the natural circulation flow rate around the lower head of the reactor vessel. For an elaborate prediction of the natural circulation flow rate using a thermal-hydraulic system code, MARS-KS1.5, a three-dimensional computational fluid dynamics (CFD) simulation is conducted to estimate the flow rate and pressure distribution of a liquid-state coolant at the brink of significant void generation. The CFD calculation results are used to determine the loss coefficient at major flow junctions, where substantial pressure losses are expected, in the nodalization scheme of the MARS-KS code such that the single-phase flow rate is the same as that predicted via CFD simulations. Subsequently, the MARS-KS analysis is performed for the two-phase natural circulation regime, and the transient behavior of the main thermal-hydraulic variables is investigated.

1. Introduction

In-vessel retention is a severe accident mitigation strategy to stabilize the core melt relocated to the lower head of the reactor vessel by flooding the reactor cavity and submerging the reactor vessel [1]. It aims to contain the molten core debris inside the reactor vessel by cooling its external surface via the natural circulation of cooling water, as illustrated in Fig. 1. In the Republic of Korea, in-vessel retention is implemented to severe accident scenarios of an up-to-date high-power reactor, APR1400; operating Shin-Kori Units 3 & 4 and Shin-Hanul Units 1 & 2, and Shin-Kori Units 5 & 6 under construction (as of 2021) belong to this type. Because the APR1400 deploys thermal insulation around the reactor vessel, a natural circulation flow circuit is established along the inner annular gap between the reactor vessel and insulation, and an outer circulation flow circuit is established between the insulation and reactor cavity wall under external reactor vessel cooling.

In APR1400, once the core exit temperature exceeds 1200 °C, the reactor cavity flooding system will initiate the supply of cooling water from the in-containment refueling storage tank (IRWST) using a shutdown cooling pump [2]. Once the molten core is relocated to the lower head, massive thermal loading is imposed on the reactor vessel wall to apply a high heat flux to the surrounding cooling water. This causes an upward natural convective flow of the cooling water in the annular channel between the reactor vessel and insulation. The continued loss of subcooling of the cooling water results in vigorous vapor generation on the lower head to form a steam/water mixture, which is then discharged through outlets embedded in the side wall of the insulation. Subsequently, the water separated from the mixture flows downward along the outer annular gap and recirculates.

If the heat transferred across the lower head is not removed appropriately, then the structural integrity of the reactor vessel will be compromised and complicated ex-vessel phenomena will occur, including fuel–coolant interactions. From a thermal viewpoint, the principal failure mechanism of the lower head is the occurrence of the boiling crisis [1]. It is well known that the critical heat flux (CHF) on a heated surface is closely associated with the mass flux of

* Corresponding author.
E-mail address: yeongun2@jejunu.ac.kr (Y.-G. Lee).

https://doi.org/10.1016/j.net.2021.07.037

NOMENCLATURE

A	Cross-sectional area (m^2)
g	Gravitational acceleration (m/s^2)
G	Mass flux (kg/m^2s)
K	Loss coefficient
$\dot{m}$	Mass flow rate ($kg\ s^{-1}$)
P	Pressure (Pa)
P_f	Wetted perimeter (m)
T	Temperature (K)
z	Coordinate (m)
β	Thermal expansion coefficient (K^{-1})
ΔP	Pressure drop (Pa)
θ	Angle of inclination (degree)
ρ	Density ($kg\ m^{-3}$)
ρ'	Momentum density ($kg\ m^{-3}$)
τ_w	Wall shear stress ($N\ m^{-2}$)
s	
fr	Frictional
g	Gravitational
I	Inlet
O	Outlet
ref	Reference
sa	Spatial acceleration
ta	Temporal acceleration

the fluid [3]. On the downward-facing hemisphere, it is revealed experimentally that the flow rate affects the CHF, particularly in the uppermost section where the thermal loads are the highest in the in-vessel retention condition [4]. Therefore, the elaborate prediction of the natural circulation flow rate is crucial for evaluating the thermal margin of external reactor vessel cooling.

Park et al. [5] performed a numerical analysis of the two-phase natural circulation flow under the external reactor vessel cooling of the APR1400. The coolant mass flow rate along the annular gap between the reactor vessel wall and insulation was calculated using the RELAP5/MOD3 code, and the sensitivity of the injection temperature of the cooling water and the initial water level was evaluated. Lim et al. [6] used MELCOR2.1, an integral code for severe accident analysis, to simulate the core degradation process and heat transfer around the lower plenum of the APR1400 in response to large-break loss-of-coolant accidents (LOCAs). However, the heat transfer coefficient and the CHF on the ex-vessel wall were calculated using pool boiling models; hence, the effect of the flow rate could not be addressed.

Whereas one-dimensional thermal-hydraulic system codes can provide accurate predictions for most two-phase flow problems, their calculation results for the natural circulation flow rate may differ substantially depending on the user's modeling scheme because free convection is generally driven by extremely small pressure differences. This applies particularly to complex-shaped flow paths such as the annular channel between the lower head and insulation, as well as the ingress and egress doors of the insulation. Meanwhile, commercial computational fluid dynamics (CFD) codes ensure higher fidelity when simulating single-phase flows, even in channels with complicated geometries, whereas its accuracy in the two-phase flow condition must be further assessed.

In this study, a two-step approach was introduced to reliably estimate the two-phase natural circulation flow rate of the APR1400 under external reactor vessel cooling using a domestic safety analysis code, MARS-KS version 1.5 [7], facilitated by CFD analyses. To compensate for the limitation of the system-scale code to fully describe complicated flow channels, the natural convective flow circuit in the reactor cavity of the APR1400 was initially modeled via the CFD code to estimate the flow rate and pressure distribution of a liquid-state coolant before significant void generation. The CFD calculation results were used to determine the loss coefficient at the dominant minor loss points in the nodalization scheme of the MARS-KS code such that the single-phase flow rate was the same as that predicted via CFD simulations. By applying the obtained loss coefficients in the single-phase liquid state, the evolution of the thermal-hydraulic variables to the two-phase natural circulation flow conditions was investigated using the MARS-KS code.

2. Problem statement

This section presents the geometric characteristics of the natural convective flow paths in the reactor cavity of the APR1400 and the initial and boundary conditions for the numerical simulation. As illustrated in Fig. 1, the side wall of the insulation was inclined in the vicinity of the lower head, and the cross-sectional flow rate was the minimum at the upper section of the hemisphere, where the heat flux from the light metal layer of the relocated corium is expected to be extremely high, thereby affording a faster fluid flow.

A hinge-type ingress door was installed at the bottom of the insulation to allow the cooling water to enter the inner space of the insulation once the reactor cavity is flooded. Most of the ingress doors were arranged repeatedly in the azimuthal direction near the periphery of the bottom of the insulation, as illustrated in Fig. 2. Owing to the relatively small cross-sectional area, the fluid flow may undergo considerable pressure loss through the ingress openings. The egress doors at the side wall of the insulation were designed such that any steam/water mixture formed around the lower head can escape to the outer annular gap between the insulation and reactor cavity wall. Furthermore, the egress doors were hinge-type doors that comprise three groups, depending on their dimensions.

The problem evaluated in this study was assumed to be a quasi-steady phenomenon. In real severe accident conditions, the accumulated volume and configuration of the molten corium in the lower head and the corresponding profile of the thermal load along the wall change over time. For simplicity, however, we assumed that the debris pool reached a steady thermal state, and that the lower head was fully submerged at the initial moment of the simulation. The initial water level was assumed to be located at the bottom-most elevation of the cold leg, and the initial water temperature was set to 48.9 °C.

To analyze the free convection in the reactor cavity, two important boundary conditions must be specified. The first is the containment pressure applied to the free surface of cavity water. This is determined by the progress of the initiating accident and the elapsed time until the relocation of the molten corium. For the current study, we referred to prior studies to evaluate the spray effect on the behavior of hydrogen in the APR1400 containment during severe accidents using the GASFLOW code [8]. The transient responses of the containment pressure to the hypothetical small-break and large-break LOCAs were calculated. It was discovered that, provided that no spray system was available during the large-break LOCA, the containment pressure reached 380 kPa in 1 h and then continued to decrease to 250 kPa at 10,000 s. Therefore, we set 250 kPa as the atmospheric pressure of the containment.

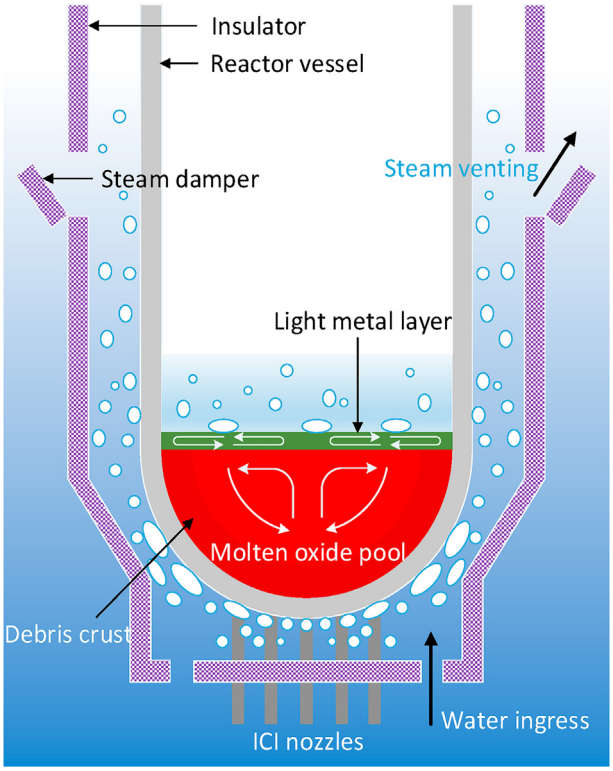

Fig. 1. Concept of external reactor vessel cooling for in-vessel melt retention.

Another crucial boundary condition was the heat flux on the ex-vessel wall of the lower head. Generally, the heat flux from the molten corium increases with the polar angle on the lower head, and the highest thermal loads are generated from the side of the light metal layer floating on the oxide pool—this is known as the focusing effect [9]. In this study, the heat flux profile calculated by the MAAP4 code [10] for the core degradation scenario of APR1400 initiated by the large-break LOCA was applied to the ex-vessel wall of the lower head, as shown in Fig. 3. A light metal layer was formed over the region of 79.1°–88.3° when a maximum heat flux of 1.27 MW/m^2 was applied. The overall thermal load was 23.3 MW.

Even though the reactor vessel was successfully flooded in the early phase of core degradation, the heat transfer from the molten core resulted in the continuous evaporation of the cooling water. Without the coolant makeup to compensate for the loss of the inventory, the water level will be lowered to below the egress door; consequently, natural circulation cooling will cease. To prevent the depletion of cavity water, the APR1400 was equipped with a boric acid makeup pump (BAMP), which supplies cooling water from the IRWST at a designated flow rate of 38.6 m^3/h (170 GPM) once it is actuated manually by an operator [2]. In the simulation of the MARS-KS code, it was assumed that the operator began supplying the coolant to the lower part of the reactor cavity once the collapsed water level lowered to 0.91 m lower than the horizontal centerline of the hot legs.

3. Three-dimensional CFD analysis

3.1. CFD model setup

A CFD study was performed for the fluid region around the reactor vessel of the APR1400. By modeling every shape of the flow channels during external reactor vessel cooling, the circulation flow rate and the pressure distribution in the fluid region in the single-phase liquid state were obtained. Furthermore, the CFD model calculated the conductive heat transfer in the solid structure, such as the reactor vessel wall, and the conjugate heat transfer in the fluid region to which heat was transferred from the lower head wall. A quarter of the flow region with quasi-symmetry geometry around the reactor vessel was modeled for an efficient computation.

The modeled geometry of the natural circulation flow channel is shown in Fig. 4. The top of the fluid region was set as a wall to create a closed circuit in the reactor cavity. This is based on the assumption that the momentum loss at the free surface is negligible, and that almost all flows are formed through ingress and egress doors. This geometry is adequate for obtaining the pressure drop through the local flow path around the reactor vessel. The in-core instrumentation nozzles installed at the bottom of the lower head wall were also modeled, as they induced flow resistances and complicated the flow field around the lower head. Note that it was assumed ingress and egress doors are fully open during flow circulation, and the simulation herein did not take into account effect of flaps which cause a complex flow pattern and results in a higher resistance in the actual situation.

A commercial CFD code, ANSYS CFX-17, was used in the simulation [11]. CFX-17 can solve the conjugate heat transfer with a turbulent flow. The large Reynolds number owing to the considerable length scale of the flow path necessitates a turbulence model. For modeling turbulent flows, the standard k–ε model was used with the scalable wall function. Additionally, the Boussinesq model was introduced to add a buoyant momentum source for the fluid [11]. The Boussinesq model calculates the density of water using the temperature difference from the reference temperature, which was set to 25 °C in the simulation, as follows:

$$\rho - \rho_{ref} = -\rho_{ref}\beta\left(T - T_{ref}\right) \quad (1)$$

where the value of the thermal expansion coefficient, β, was 2.57 10^{-4}/K.

A mesh system was constructed for the fluid region between the reactor vessel and reactor cavity, as shown in Fig. 5. The total number of elements in the mesh system was 2.4 million. A hexahedral mesh was used for the reactor vessel wall, except for the lowest part of the lower head. All fluid regions were modeled with a hexahedral mesh. Meshes near the wall were set exhibit an exponential increment of 1.4 to resolve the boundary layer. Each mesh part was connected using the general grid interface option to correct unmatched grid points. y^+ values were 6 and 14 at ingress and egress openings, respectively, where complicated flow structures are expected.

The boundary conditions implemented in this CFD model are shown in Fig. 4. An adiabatic condition was applied to the wall of the fluid region. Symmetric conditions were implemented on the side planes of the fluid region and structures. The heat flux profile was imposed on the inner surface of the lower head wall, as shown in Fig. 3. The reference pressure of the system was set to 380 kPa such that the hydrostatic pressure at the top of the fluid region can be maintained at 250 kPa, and the initial temperature was 322.05 K.

The entire simulation was conducted in the transient mode to investigate temporal changes in the temperature and velocity of the cooling water. The time step was set to 4 s, and ten iterations were allowed for each time step. The root-mean-square (RMS) of the residuals of momentum, pressure, and solid and fluid energies was monitored, as shown in Fig. 6. The plots show that the RMS of the residual of momentum was maintained around 10^{-4}, and that of the energy and pressure were less than 10^{-4}.

The mesh size sensitivity was investigated by using ‘coarse’ meshes with 1.3 M elements, and ‘fine’ meshes mentioned above.

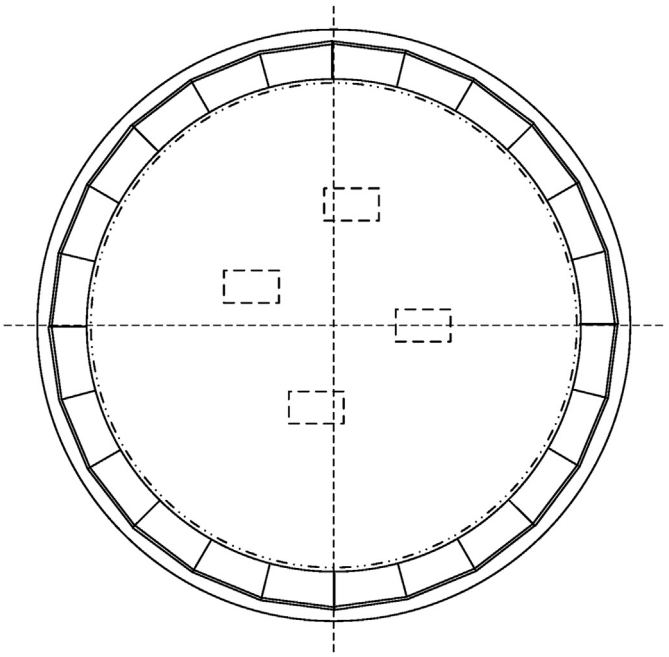

Fig. 2. Configuration of ingress doors at bottom of thermal insulation.

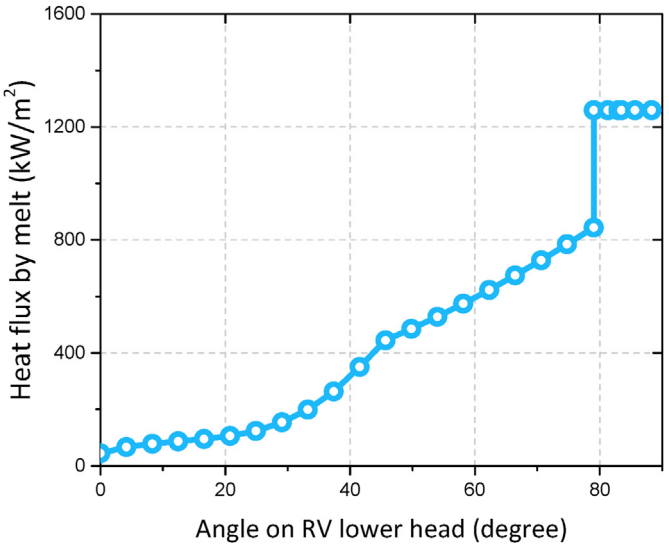

Fig. 3. Heat flux profile by relocated core melt on lower head wall based on polar angle.

The average exit temperature (temperature at egress openings) was compared when the mean temperature at ingress openings was 331 K for both mesh systems. As summarized in Table 1, the difference in the average temperature at egress openings was less than 0.27 %, which indicates that the applied mesh system is refined enough.

3.2. CFD calculation results

According to the preliminary analysis of MARS-KS, significant vapor generation commenced on the lower head wall as the inflow temperature of cooling water reached 382 K (see Section 4.2.1). To compare the calculation results from the two codes in the absence of the vapor phase, the CFD simulation was continued until the average fluid temperature at the ingress passages reached 382 K.

The temperature and axial velocity (w) distributions of the cooling water at the ingress openings were plotted, as shown in Fig. 7. Both the temperature and the axial velocity had larger values across openings around the periphery of the insulation than in the middle passages because a larger flow rate was established through a shorter flow path. Furthermore, it was discovered that, because of the different cross-sectional areas of the egress doors, the temperature profile of the inflow of cooling water was non-uniform in the azimuthal direction. At that instant, the mass flow rate across the ingress doors in the quarter was approximately 60.5 kg/s, yielding a total rate of 242 kg/s through the entire opening.

Fig. 8 presents the flow streamline over the cross-plane that passes through the center of an egress door. This figure shows several notable flow characteristics in the fluid region. The fluid experienced a buoyant force near the lower head of the reactor vessel, where a high heat flux was applied. Subsequently, the water rose upward and passed through the egress doors. A large vortex flow was generated at the outer space of the egress doors owing to the high local velocity of the fluid and its impingement on the reactor cavity wall. Part of the fluid moved downward along the narrow passages between the insulation and reactor cavity. However, the descending flow could not penetrate deep into the bulk of water in the lower reactor cavity, which served as an isolated section with delayed mixing.

The velocity and absolute pressure distributions in the flow region are shown in Fig. 9. The calculation results indicated that strong flows formed at the ingress openings, egress passages, and narrow channels between the lower insulation and reactor cavity. Therefore, a large pressure drop was expected in these regions. The absolute pressure field was extracted to estimate the loss coefficients used in the MARS-KS calculation, as shown in Fig. 9(b). Subsequently, the area-averaged value over the x–y planes were obtained at different elevations such that a one-dimensional pressure change can be generated.

4. MARS-KS models and calculation results

4.1. MARS-KS modeling

The MARS-KS nodalization of the flow channel for the external reactor vessel cooling is shown in Fig. 10. The lower section of the reactor cavity underneath the insulation was modeled as a pipe component containing four volumes (C120). The IRWST for the makeup of the cooling water in the reactor cavity was modeled by a time-dependent volume component, which was connected to the third volume of C120. The water supply via the BAMP was modeled by a time-dependent junction, C115; a designated trip was latched true when the collapsed liquid level was less than a prescribed value.

The single-volume component C210 models the non-heating section between the insulation and the bottom of the reactor vessel. The single-junction component C205 represents the ingress openings at the bottom of the insulation connecting C120 to C205. The annular gap between the lower head of the reactor vessel and the insulation was modeled as three annulus components, to which the thermal loads by the molten corium were applied. C220 and C240 comprised two volumes, whereas C230 was partitioned into four volumes. Heat structures were provided at these hydrodynamic volumes in the heating section to implement the boundary conditions for the surface heat flux. In other words, the heat flux inputs were assigned to eight intervals based on the lower head angle.

Since most egress openings are located along the periphery of the bottom of the insulation, the main stream of cooling water

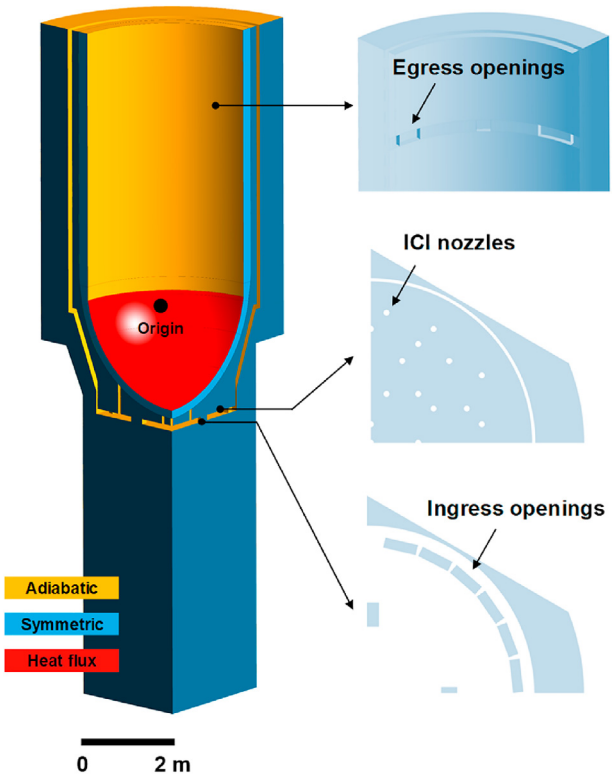

Fig. 4. Computational geometry and boundary conditions for three-dimensional CFD analysis.

entering through ingress doors can be considered vertically upward. Hence, the inclination angles for hydrodynamic nodes between the lower head and the insulation were given as 90°. That is, the cell elevation change used for calculations of the gravity head was equal to the cell length in C220 – C240, and the flow regime was evaluated based on the embedded flow regime map for vertical flows.

The annular channel between the cylindrical body of the reactor vessel and the insulation was modeled as pipe components C310 and C320, which comprised ten and eight volumes, respectively. Connected to the exit of the seventh volume of C310 was cross junction C345, which represented egress doors that allowed the release of the steam–water mixture from the insulation. Another cross junction, C355, was used to simulate steam dampers above the hot legs. The exit of the annular channel C320 was connected to a time-dependent volume that modeled the free volume of the reactor containment.

The outer annular gap between the insulation and reactor cavity wall was modeled by annulus components C410 and C420, each containing ten and four volumes, respectively. During external reactor vessel cooling, the cooling water flowed downward through C410 and C420 to the lower section of the reactor cavity. The outer annular gap above the bottom of the hot legs was modeled as annulus component C510, which was connected to a time-dependent volume for the containment atmosphere. Steam generated from the lower head was discharged primarily from C510 to C520.

4.2. Loss coefficients of flow channels

4.2.1. Simulations without loss coefficients

The minor losses arising from changes in the flow area or the entrance/exit effects significantly affected the circulation flow rate under free-convection conditions. Because the flow paths of the external reactor vessel cooling exhibited frequent variations in the cross-sectional area and flow direction, an appropriate estimation of loss coefficients is crucial for performing a one-dimensional system-scale analysis employing large control volumes. Generally, the loss coefficient for a specific geometry is empirically obtained by controlling the flow velocity. However, this is not applicable to prototypical annular channels in the reactor cavity; therefore, we estimated the loss coefficients based on the high-fidelity CFD analysis results.

To perform a comparison with the CFD calculation results, a preliminary MARS-KS simulation was first conducted no loss coefficient provided to the flow junctions. The calculation results of the natural circulation flow rate are presented in Fig. 11. The temperature of the cooling water continued to increase owing to the heat loads from the relocated corium, and the flow rate increased significantly once the transition to the two-phase natural circulation regime occurred. The free-convective flow exhibited considerable oscillations as the cooling water approached the saturation state; however, the oscillations stabilized at a flow rate of approximately 3900 kg/s after 8400 s. This value is approximately three times the flow rate estimated in a preceding study by Park et al. for the APR1400 [5], indicating that the predicted circulating flow rate may vary substantially depending on the implemented loss coefficients.

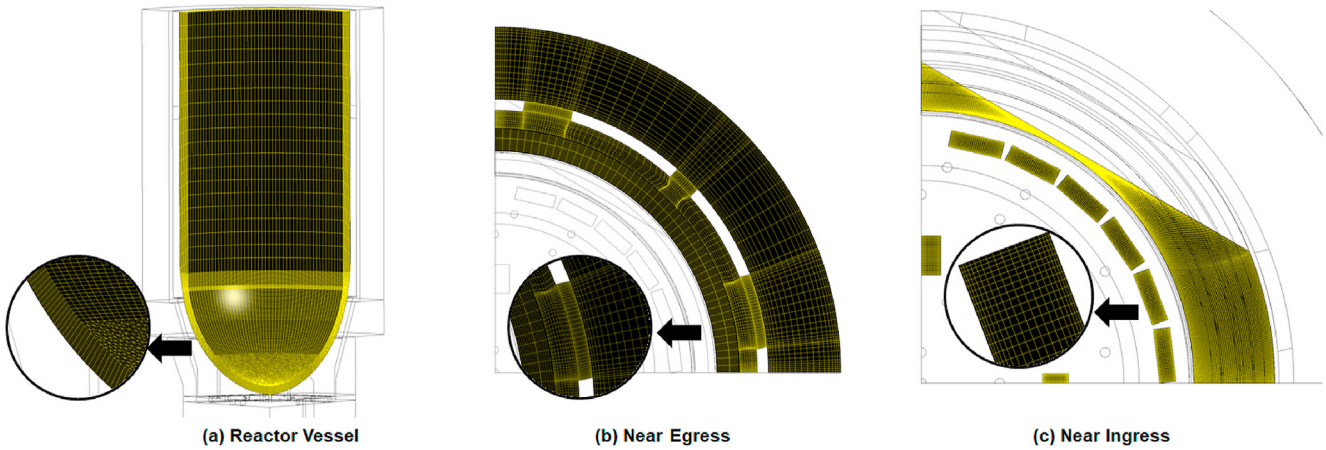

Fig. 5. Computational mesh structure.

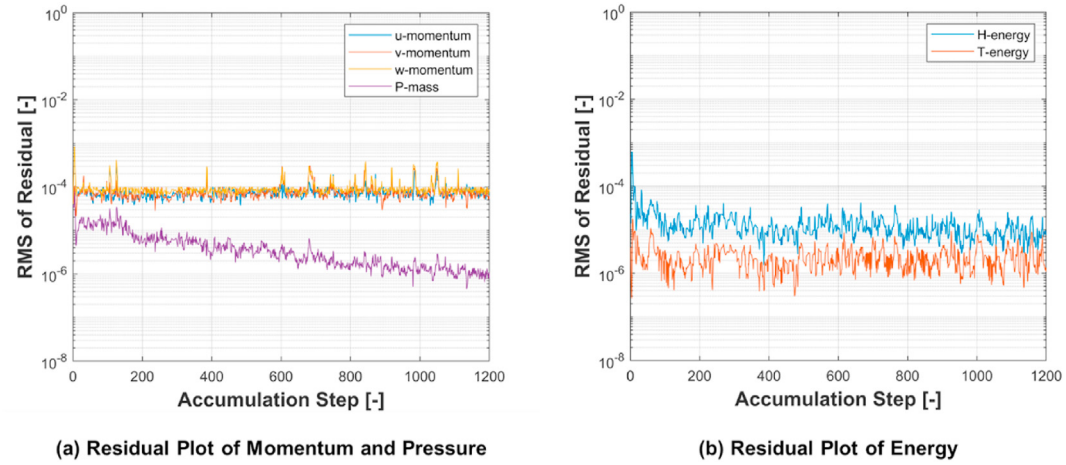

(a) Residual Plot of Momentum and Pressure (b) Residual Plot of Energy

Fig. 6. RMS of residuals of momentum, pressure, and energy.

Table 1
Mesh sensitivity result for natural circulation.

Types	Number of meshes (fluid/solid)	Mean temperature at ingress openings (K)	Mean temperature at egress openings (K)
Coarse	1,342,660 (1,306,550/36,110)	331.011	339.547
Fine	2,480,779 (2,305,995/174,784)	331.139	340.482

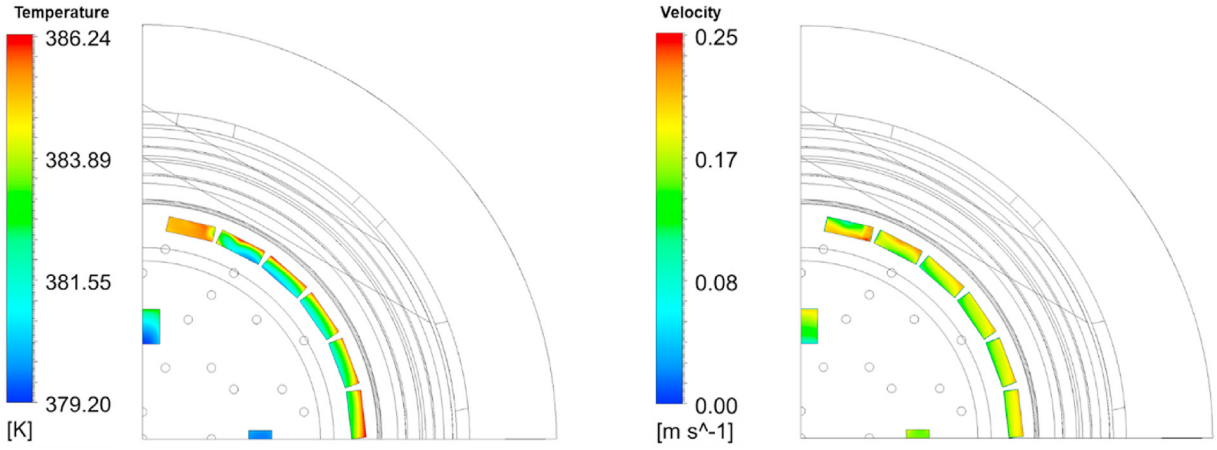

(a) Ingress Temperature Distribution (b) Ingress Velocity Distribution

Fig. 7. Temperature and axial velocity distributions at ingress openings.

In this study, we estimated the loss coefficients based on the CFD calculation results obtained at the brink of significant void generation on the lower head of the reactor vessel. Fig. 12 shows the calculated variation of the void fraction at hydrodynamic volumes in the heating section. At the second node of C240, where the surface heat flux was the highest and the liquid subcooling degree was minimum, the void fraction began to increase significantly at approximately 1750 s. One may assume that the transition is initiated from the single-phase to the two-phase natural circulation regime at this instant; hence, the transition was designated as the point for comparing the calculation results of the MARS-KS code with the aforementioned CFD analysis results. The inlet temperature of the cooling water into the inner annular gap was 382 K at this instant, and the circulation flow rate from the CFD analysis corresponding to this temperature was approximately 242 kg/s.

4.2.2. Estimation of loss coefficients

The expression for the pressure gradient of a two-phase mixture comprises acceleration, gravitational, and frictional terms, as follows [12]:

$$\left(-\frac{\partial P}{\partial z}\right) = \left(-\frac{\partial P}{\partial z}\right)_{ta} + \left(-\frac{\partial P}{\partial z}\right)_{sa} + \left(-\frac{\partial P}{\partial z}\right)_{g} + \left(-\frac{\partial P}{\partial z}\right)_{fr} = \frac{\partial G}{\partial t} + \frac{1}{A}\frac{\partial}{\partial z}\left(\frac{G^2 A}{\rho'}\right) + \rho g \sin\theta + \frac{\tau_w P_f}{A} \quad (2)$$

Here, the acceleration pressure loss includes both temporal and spatial acceleration terms. The integration of Eq. (2) along a pipe system results in minor pressure drops caused by abrupt changes in the flow area, flow direction, etc.

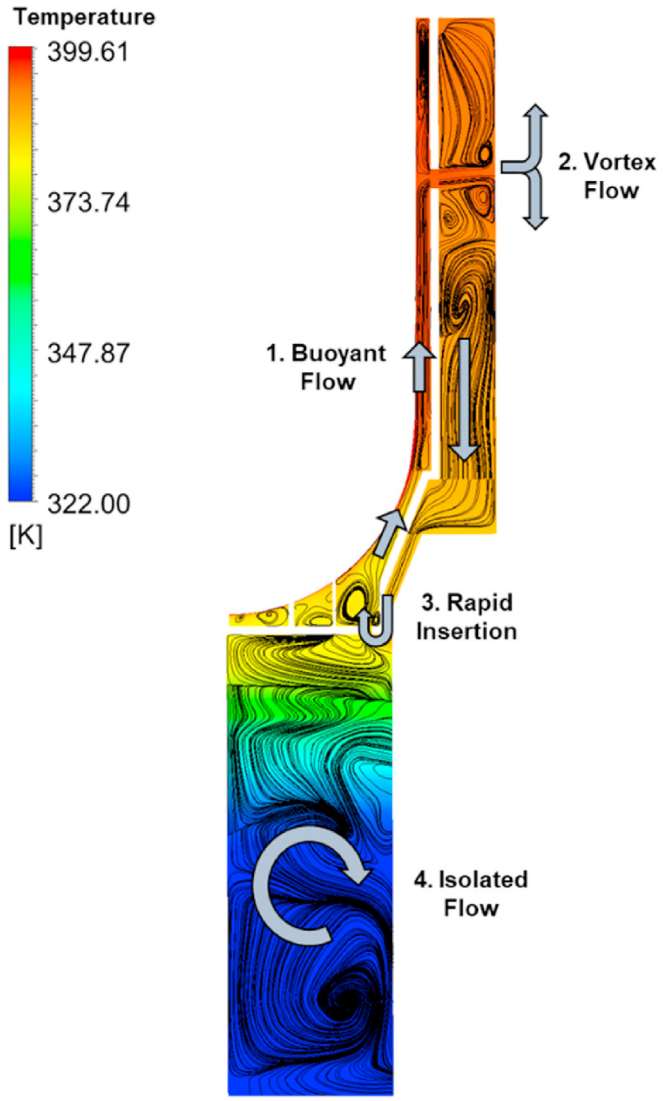

Fig. 8. Flow streamline with temperature contour.

$$P_I - P_O = \int_{P_I}^{P_O} \left\{ \left(-\frac{\partial P}{\partial z} \right)_{ta} + \left(-\frac{\partial P}{\partial z} \right)_{sa} + \left(-\frac{\partial P}{\partial z} \right)_{g} + \left(-\frac{\partial P}{\partial z} \right)_{fr} \right\} dz + \sum_{j=1}^{N} \Delta P_j \tag{3}$$

where ΔP_j indicates the total pressure drop due to flow disturbance at junction j. The form pressure drop in Eq. (3) is expressed as follows:

$$\Delta P_j = K_j \frac{\dot{m}_j^2}{2\rho A_j^2} \tag{4}$$

When no loss coefficient is provided to the input model of MARS-KS, the pressure drop due to minor losses is zero. Hence, the total pressure drop between the two points is expected to be larger in the CFD analysis than that in the MARS-KS calculation excluding the minor losses, provided that the flow conditions are the same. In other words, the total pressure drop across an interval calculated using the CFD code will deviate from that obtained using MARS-KS by as much as the minor pressure drop, and one can obtain the loss coefficient based on the difference in the calculated pressure drops from the two codes. As shown in Eq. (3), not only the minor loss terms, but also other pressure drop terms rely on the flow rate. Therefore, we estimated the loss coefficient at a junction as follows:

(1) Based on trial-and-error, a large loss coefficient was imposed on an arbitrary single junction such that the flow rate of cooling water calculated via MARS-KS was equal to that obtained from the CFD analysis (242 kg/s) when the inlet temperature to the inner annular gap reached 382 K. This was performed to compare the total pressure drops from the two codes, while maintaining identical pressure loss terms except for the minor loss terms.
(2) The pressure drop at a specific junction (the pressure difference between two adjoining nodes) was extracted from the calculation results using the CFD and MARS-KS codes. For the CFD analysis, the cross-section-averaged pressure at the center of a node was utilized.
(3) The loss coefficient was estimated based on the difference in the calculated pressure drops from the two codes as follows:

$$\Delta P_{j\_CFD} - \Delta P_{j\_MARS} = K_j \cdot \frac{1}{2} \frac{\dot{m}_j^2}{\rho A_j^2} \tag{5}$$

(4) The procedures above were repeated for all junctions, at which a significant minor pressure drop was anticipated. All the obtained loss coefficients were provided in the MARS-KS input deck, and a new simulation was performed in the two-phase natural convection regime.

In this study, based on a detailed investigation of the geometric characteristics of natural convective flow paths in the reactor cavity of the APR1400, it was inferred that a significant minor pressure drop would occur in three sections: the ingress doors and the lower region of the inner annular gap (section A), the egress doors at the insulation (section B), and the downward channel between the lower part of the insulation and reactor cavity wall, accompanied by an abrupt contraction in the flow area (section C), as illustrated in Fig. 13. With regard to the vertical flow channels, i.e., sections A and C, the calculated total pressure drops along the hydrodynamic domain were applied to Eq. (5) to estimate the loss coefficient at a single junction with the minimum flow area.

For the egress doors region, however, the mean flow velocity and pressure loss were dissimilar for each opening in the calculation results of the CFD code because the three types of egress doors had different opening areas; hence, a non-symmetric multi-dimensional flow structure was created around the egress doors. Moreover, the flow separation arising from the impingement of the cooling water on the reactor cavity wall (see Fig. 8) rendered it difficult to define an appropriate surface or line to extract the pressure field. In other words, because the MARS-KS models three different-sized groups of egress doors via a single cross-junction, it is uncertain how one can represent a reference velocity or the pressure drop across 12 egress doors for a one-dimensional modeling approach. Applying the arithmetic mean would be inappropriate. Therefore, instead of using the differences in the calculated pressure drop between the codes, we employed an iterative method to obtain the loss coefficient for the egress doors

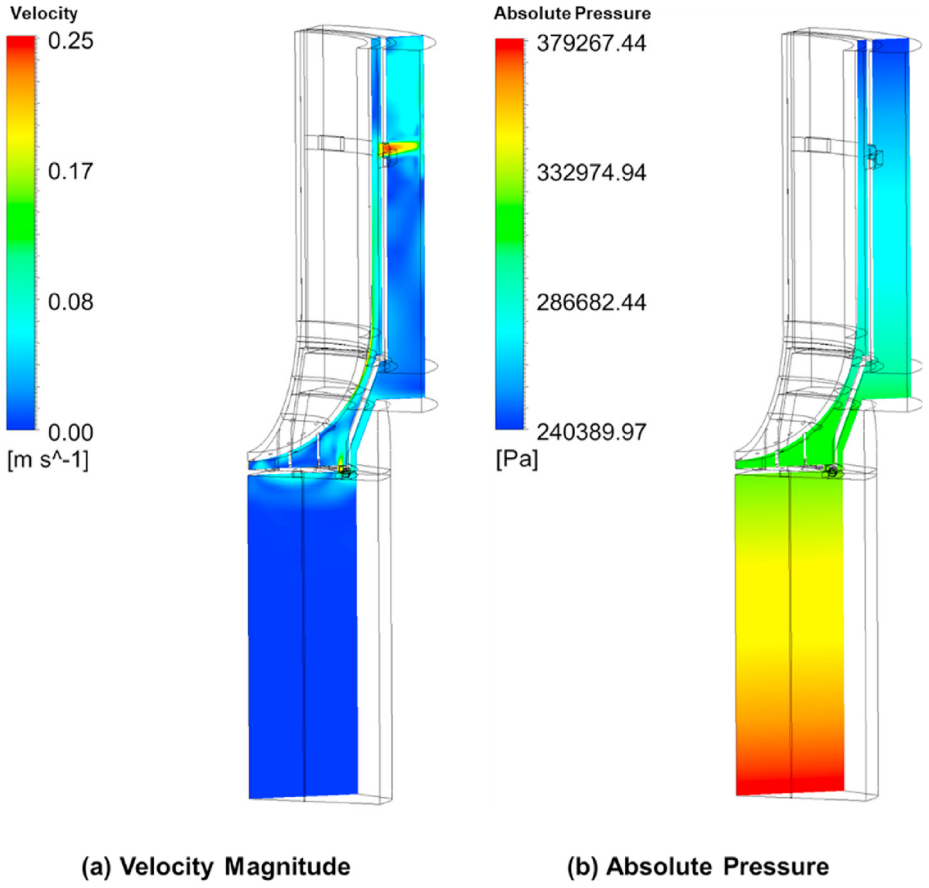

Fig. 9. Velocity and absolute pressure distribution at center plane.

that rendered the flow rate in the MARS-KS model the same as that predicted by the CFD simulation at the instant of comparison. The obtained form loss coefficients for three sections were summarized in Table 2.

4.3. Simulation results

The loss coefficients deduced from the CFD-aided estimation above were assigned to the input model of the external reactor vessel cooling, and the two-phase natural circulation flow was re-evaluated. The simulation was performed for 10,000 s, and the calculation results are shown in Figs. 14–19.

Fig. 14 presents the transient behavior of the cooling water temperature around the lower head of the reactor vessel. As high thermal loads were applied to the cooling channel, the cooling water reached the saturation state at approximately 2400 s, and a number of vapor bubbles were generated in the nucleate boiling regime. The collapsed water levels inside and outside the insulation are shown in Fig. 15. Initially, the water level increased by the heating up of the cooling water, and the vapor generation rate increased significantly around the saturation temperature. As the cooling water vaporized at a rate analogous to the heat load from the lower head, steam was released to the atmosphere of the reactor containment (C330 or C520), and the water level decreased continuously until the BAMP was actuated.

The collapsed water level inside the insulation became lower than that outside the insulation because of vigorous vapor generation on the surface of the lower head from 2000 s. On the contrary, the volumes in the outer annulus below the elevation of egress openings were filled with water while vapors entering through egress openings flowed upward and discharged into the upper free volume simulated by C520. This difference of collapsed water levels between inside and outside the insulation represents the difference in hydrostatic heads between upward and downward flow channels, which acts to the driving force of natural circulation around the insulation.

The variation in the natural circulation flow rate across the ingress doors is shown in Fig. 16. The mass flow rate did not exceed 350 kg/s in the liquid state; however, it increased significantly as the cooling water reached the saturation state. This is because the steam bubbles generated on the lower head were accelerated by the buoyancy force and entrained the surrounding water owing to the interfacial drag. The flow rate oscillated significantly during the initial phase of the transition into the two-phase natural circulation regime; however, it stabilized immediately after. For the ingress doors at the bottom of the insulation, the total circulation rate by free convection was approximately 870 kg/s, and the corresponding flow velocity was 0.51 m/s. The water–steam mixture from the inner annular gap was discharged through the cross-junction at a lower elevation (C345), whereas the circulation flow rate across the upper steam damper (C355) was almost negligible. Note that form loss coefficients used in the MARS-KS code were the Reynolds number independent values, and thus their variation versus the flow velocity were not taken into account; this approach may cause a higher resistance in the simulation, considering that a loss coefficient tends to decrease with the Reynolds number.

The coolant makeup was initiated at 4893 s when the collapsed water level was lowered to the set point for the actuation of the

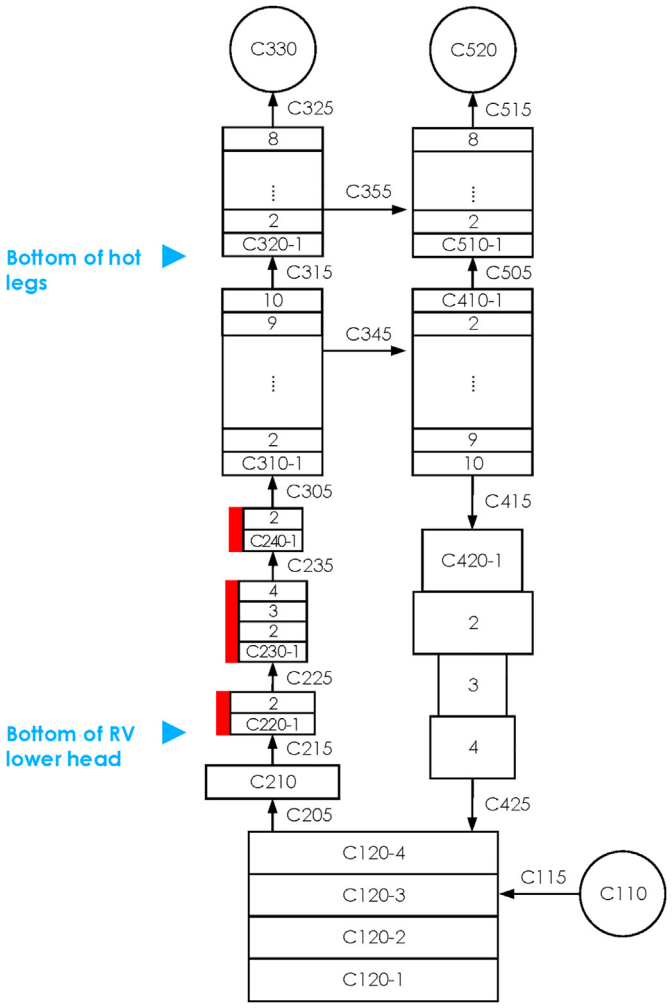

Fig. 10. Nodalization of natural circulation flow channels during external reactor vessel cooling.

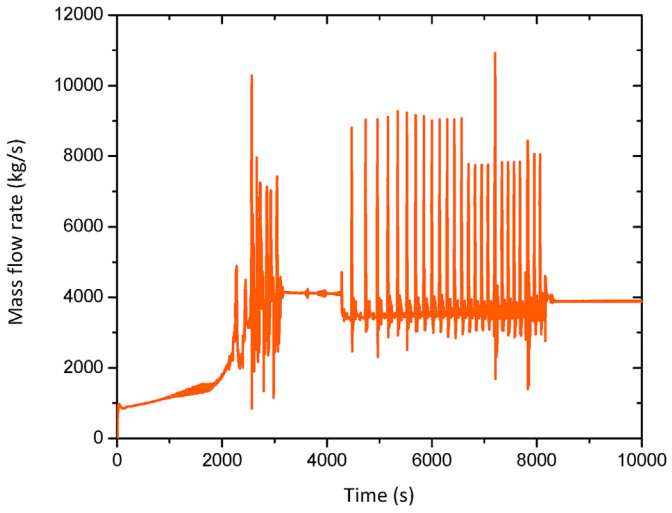

Fig. 11. Calculated natural circulation flow rate without loss coefficients.

BAMP. Owing to the continuous supply of cooling water from the IRWST, the total inventory inside the reactor cavity can be preserved. Because the coolant makeup rate was slightly larger than

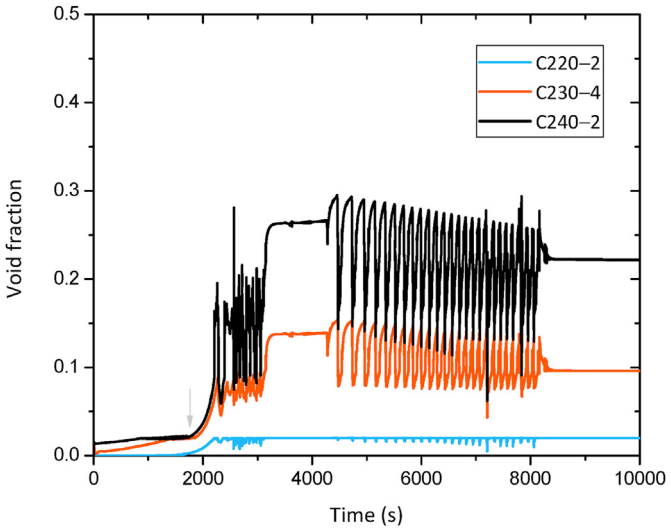

Fig. 12. Calculated void fraction around lower head wall without loss coefficients.

the water evaporation rate by the core melt, the water level increased gradually, as shown in Fig. 15. Unless additional cooling water can be provided from an external source, the water level will continue to decrease. Once the water level becomes lower than the elevation of the egress doors, the liquid circulation in a closed circuit will be completely deteriorated in 12,600 s as shown in Fig. 20, and the heat removal from the lower head will be performed under pool boiling conditions.

The changes in the void fraction at hydrodynamic volumes adjacent to the lower head and the axial profile of the void fraction along the inner annulus gap at 10,000 s are presented in Figs. 17 and 18, respectively. The cooling water introduced in the single-phase liquid state evaporated by the heat flux from the lower head surface to increase the void fraction of the water–steam mixture, and the void fraction of C240, where the heat flux from the core melt is the maximum, at the end time reached 0.5. When the water–steam mixture was released to the outer annulus gap through the egress doors, a higher ratio of steam than water moved through C345, reducing the void fraction at nodes higher than the cross-junction, as shown in Fig. 18.

Fig. 19 presents the heat transfer mode at the exterior surface of heat structure S240, to which the light metal layer in the molten core debris exerted an extremely high heat flux. As shown, the nucleate boiling regime was sustained over the entire transient time by the two-phase natural circulation flow established along the annular channels. The simulation results for convective heat transfer on the lower head, as summarized in Table 3, show that the temperature difference between the outer wall and the cooling water was less than 72 K.

This implies that the MARS-KS code forecasts that the relocated core melt of the APR1400 is coolable and retainable via the external flooding of the reactor vessel under the conditions described in Section 2. However, more deliberate considerations are required for a definite conclusion. According to the logic for determining the heat transfer mode, the MARS-KS code should consider that the transition to the post-departure from nucleate boiling regime occurs when the surface heat flux is larger than the CHF [13]. Hence, applying an adequate CHF model is crucial for evaluating the coolability limit of external reactor vessel cooling. It is noteworthy that MARS-KS does not incorporate a CHF model applicable to the downward-facing hemisphere. In the simulation, the CHF was calculated using the default model for a circular tube based on the 1986 AECL-UO CHF lookup table [14].

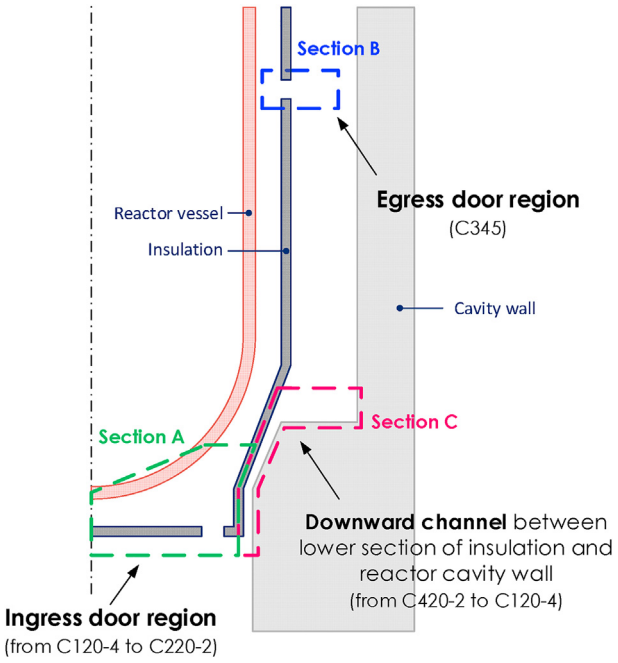

Fig. 13. Locations of significant minor pressure drops.

Table 2
Estimated loss coefficients.

Junctions	K value	Related interval in Fig. 13
C205	12.3	Section A
C345	63.0	Section B
C420-2	157	Section C

The CHF on the external vessel surface predicted by the default model ranged from 2.5 to 3.1 MW/m^2. This is much higher than the value expected for the downward-facing hemisphere, from which the release of generated vapors is obstructed [4,15,16]. Accordingly, MARS-KS predicted that the heat transfer mode was maintained at the nucleate boiling regime over the entire transient, originating from thermal loadings of 1.27 MW/m^2 at the maximum. To more accurately predict the heat transfer and thermal margins on the lower head surface during external reactor vessel cooling, a suitable CHF model for the downward-facing hemisphere must be implemented into the analysis code. This will be investigated in future studies, in addition to the reliable prediction of the free-convective flow rate.

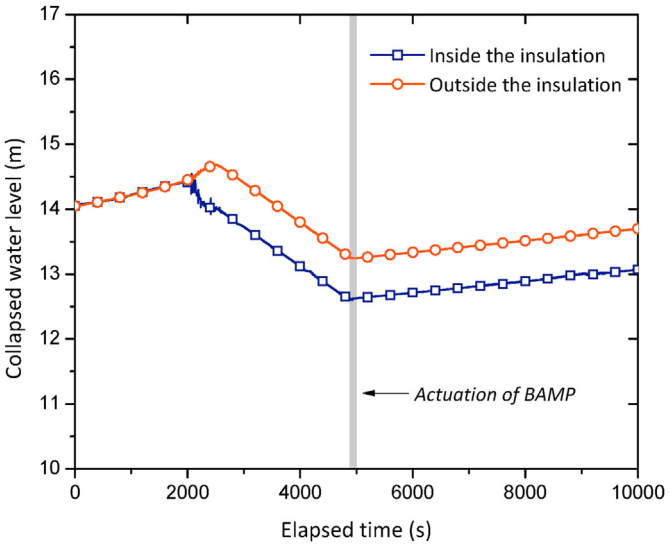

Fig. 15. Collapsed water levels at inner and outer annular gaps.

5. Conclusions

In this study, the two-phase natural circulation flow by the external reactor vessel cooling of the APR1400 was investigated numerically using the MARS-KS1.5 code based on a CFD-aided estimation of loss coefficients. Loss coefficients at three junctions with significant minor pressure drops were obtained such that the flow rate calculated by the MARS-KS code was identical to that predicted via CFD simulations in the single-phase liquid state prior to substantial vapor generation. It was revealed from the calculation that the natural circulation flow rate reached around 900 kg/s after undergoing severe flow oscillations during the transition to the two-phase regime. The coolant makeup from an external source enabled sustaining the water inventory in the reactor cavity, and

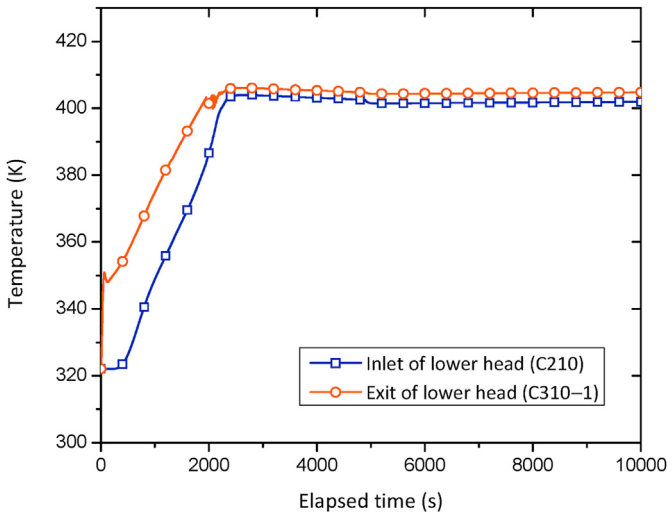

Fig. 14. Temperature of cooling water near lower head.

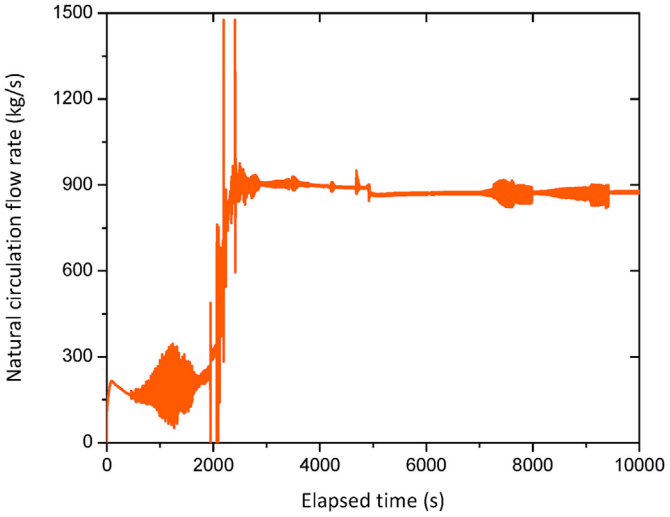

Fig. 16. Natural circulation flow rate across ingress doors.

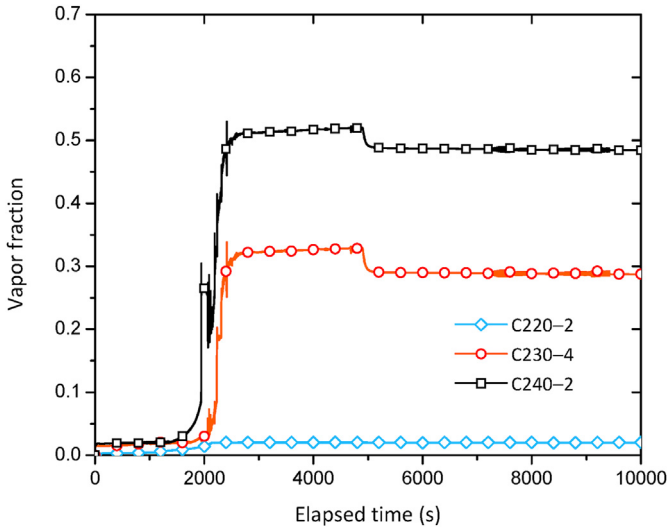

Fig. 17. Void fraction at hydrodynamic volumes adjacent to lower head.

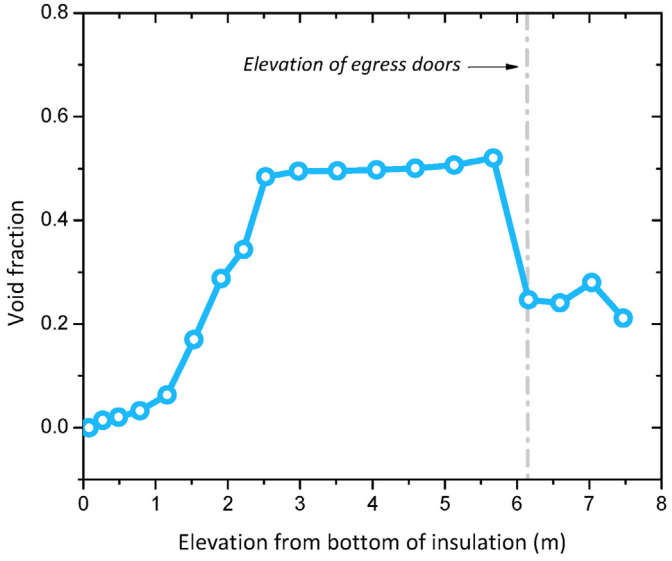

Fig. 18. Axial profile of void fraction along inner annulus gap at end time of calculations.

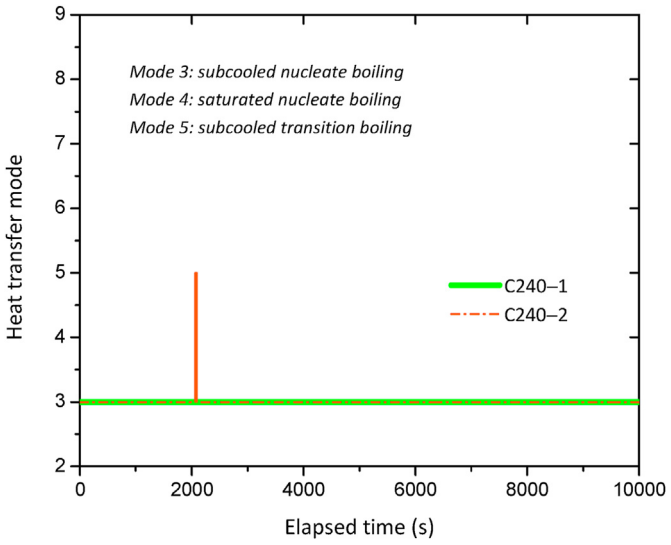

Fig. 19. Heat transfer mode at exterior surface of lower head wall.

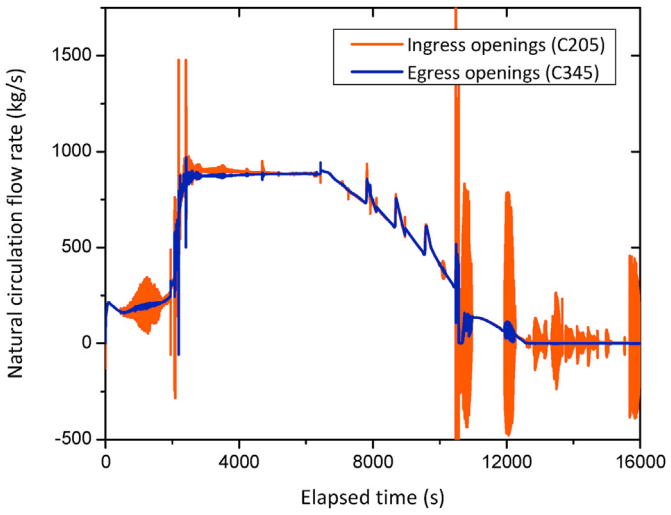

Fig. 20. Deterioration of natural circulation flow without makeup of cooling water by BAMP.

the natural circulation cooling of the reactor vessel.

In the future work, a new validated CHF correlation will be implemented into the MARS-KS code since the current version does not incorporate a proper model for the downward-facing hemisphere. As the CHF is affected by the fluid velocity around the heated surface, the results of this study will contribute to more reliable prediction of the limit of coolability to achieve in-vessel melt retention from a thermal viewpoint. Subsequently, the improved MARS-KS model will be coupled with the smoothed-particle hydrodynamics (SPH) code, named SOPHIA [17], to provide a new analysis method for the in-vessel retention of the molten core debris. Based on the meshless method, the SPH model calculates the free convective motion of the corium pool and heat loads to the lower head without relying on empirical correlations. Ultimately, we will be able to propose a novel multi-scale analysis of in-vessel melt retention, in which in-vessel corium behaviors are solved via a Lagrangian particle-based method, whereas ex-vessel cooling is predicted based on a thermal-hydraulic system code.

Declaration of competing interest

The authors declare that they have no known competing financial interests or personal relationships that could have appeared to influence the work reported in this paper.

Table 3
Predicted convective heat transfer coefficient (HTC) and surface temperature on lower head wall at end time of calculations.

Heat structure	Polar angle (°)	HTC (kW/m^{2}K)	Surface temperature (K)
S220	0–24.0	3.59	432
	24.0–34.2	5.11	434
S230	34.2–47.1	7.53	446
	47.1–57.7	10.1	455
	57.7–67.2	11.6	458
	67.2–76.1	13.0	461
S240	76.1–81.7	17.0	465
	81.7–88.3	17.8	476

Acknowledgement

This work was supported by the Nuclear Safety Research Program through the Korea Foundation Of Nuclear Safety (KoFONS) using the financial resource granted by the Nuclear Safety and Security Commission (NSSC) of the Republic of Korea. (No. 1903003)

References

[1] T.G. Theofanous, C. Liu, S. Additon, S. Angelini, O. Kymäläinen, T. Salmassi, In-vessel coolability and retention of a core melt, Nucl. Eng. Des. 169 (1997) 1–48.
[2] S. Heo, J. Lee, Y.-C. Kang, Preliminary Design of Optimized Reactor Insulator for Severe Accident Mitigation of APR1400, Transactions of the Korean Nuclear Society Spring Meeting, Jeju, Korea, May 10-11, 2007.
[3] D.C. Groeneveld, L.K.H. Leung, P.L. Kirillov, V.P. Bobkov, I.P. Smogalev, V.N. Vinogradov, X.C. Huang, E. Royer, The 1995 look-up table for critical heat flux in tubes, Nucl. Eng. Des. 163 (1996) 1–23.
[4] T.N. Dinh, J.P. Tu, T. Salmassi, T.G. Theofanous, Limits of Coolability in the AP1000-Related ULPU-2400 Configuration V Facility, University of California, Santa Barbara, 2003. CRSS-03/06.
[5] R.J. Park, K.S. Ha, H.Y. Kim, Detailed evaluation of natural circulation mass flow rate in the annular gap between the outer reactor vessel wall and insulation under IVR-ERVC, Ann. Nucl. Energy 89 (2016) 50–55.
[6] K. Lim, Y. Cho, S. Whang, H.S. Park, Evaluation of an IVR-ERVC strategy for a high power reactor using MELCOR 2.1, Ann. Nucl. Energy 109 (2017) 337–349.
[7] J.-J. Jeong, K.S. Ha, B.D. Chung, W.J. Lee, Development of a multi-dimensional thermal-hydraulic system code, MARS 1.3. 1, Ann. Nucl. Energy 26 (1999) 1611–1642.
[8] J. Kim, U. Lee, S.W. Hong, S.B. Kim, H.D. Kim, Spray effect on the behavior of hydrogen during severe accidents by a loss-of-coolant in the APR1400 containment, Int. Commun. Heat Mass Tran. 33 (2006) 1207–1216.
[9] B.R. Sehgal, Nuclear Safety in Light Water Reactors: Severe Accident Phenomenology, Academic Press, 2011.
[10] R.E. Henry, et al., MAAP4 – Modular Accident Analysis Program for LWR Power Plants, Research Project, 1994.
[11] ANSYS CFX-Solver Theory Guide, Release 14.0, ANSYS, Inc., Canonsburg, PA., 2016.
[12] S.M. Ghiaasiaan, Two-phase Flow, Boiling, and Condensation: in Conventional and Miniature Systems, Cambridge University Press, 2007.
[13] B.D. Chung, S.W. Bae, S.W. Lee, C. Yoon, M.K. Hwang, K.D. Kim, J.J. Jeong, MARS Code Manual Volume V: Models and Correlations, Korea Atomic Energy Research Institute, 2010. KAERI/TR-3872/2009.
[14] D.C. Groeneveld, S.C. Cheng, T. Doan, AECL-UO critical heat flux lookup table, Heat Tran. Eng. 7 (1986) (1986) 46–62.
[15] S. Rouge, I. Dor, G. Geffraye, Reactor Vessel External Cooling for Corium Retention SULTAN Experimental Program and Modelling with CATHARE Code, Workshop on In-Vessel Core Debris Retention and Coolability, 3–6, Garching, Germany, 1998. March.
[16] C. Iwaki, H. Sato, D. Kanamori, Development of critical heat flux correlation for in-vessel retention, J. Nucl. Sci. Technol. 57 (2020) 951–962.
[17] Y.B. Jo, S.-H. Park, H.Y. Choi, H.-W. Jung, Y.-J. Kim, E.S. Kim, SOPHIA: development of Lagrangian-based CFD code for nuclear thermal-hydraulics and safety applications, Ann. Nucl. Energy 124 (2019) 132–149.